

About electrons and position in Triplet Production: some remarks

G. O. Depaola¹, M. L. Iparraguirre¹, D. Palacios²

¹Facultad de Matemática, Astronomía y Física, Universidad Nacional de Córdoba.
Dr. Medina Allende s/n. Ciudad Universitaria. Córdoba 5008. Argentina.

²Instituto Universitario Aeronáutico. Av. Fuera Aerea. Córdoba 5000. Argentina.

E-mail: depaola@famaf.unc.edu.ar

Abstract. Taking into account the increasing interest in measuring high energy gamma ray polarization, Boldishev et. at. [1] published an extensive and very comprehensive work on the possibility of using the recoil electrons in the production of pairs on electrons. However, this work is based on using only 2 Feynmann diagrams of the 8 that the process has. This eliminates the difficulty of distinguishing, in the theory, which is the recoil electron and which is the created

In this work we have analyzed the eight Feynman diagrams and we have shown that for energies lower to $\sim 1000mc^2$, the assumption just described is not a good approximation, so we propose a different way to work [2]: we classify the electrons into the less energetic and the most energetic ones without taking into account their origin. Under these conditions (lower or higher energy value), we have calculated the contribution of the different diagrams to the distribution (we compare the sum of them with that obtained by Haug [3][4], and how these distributions are modified by introducing a threshold for the momentum detection for electrons.

For the study of polarization we presented on the angular distribution of particles for high-energy gamma rays (where only Borsellino diagrams predominate). Our results on the azimuthal distribution show that it is highly influenced by the orientation (in the plane perpendicular to the direction of the photon), prior to the interaction, that the polarization vector has with respect to the position of the electron in whose field the pair will be generated.

1. Introduction

In the present days, there are several proposals for the development of instruments to measure polarization of high energy gamma rays of extraterrestrial origin. The changes measured by INTEGRAL in the polarization direction of the CRAB nebula ([5]) in the optical range and low energy gamma rays demonstrate that the study of this characteristic can provide much relevant information.

When a high-energy gamma ray interacts with matter, it is most likely to interact with the electric field of either the atomic nucleus or an electron of the atom and become an electron-positron pair. When it does so with the atomic nucleus, given the high mass

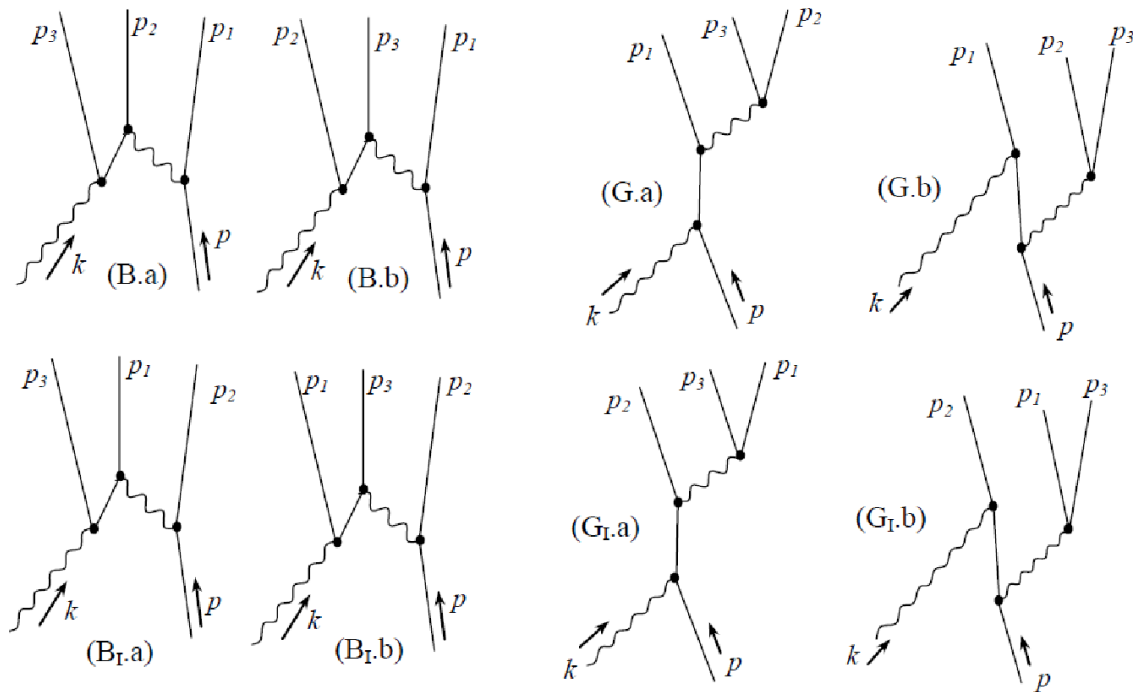


Figure 1: Feynman diagrams describing photoproduction of $e^+ e^-$ pairs on free electrons.

of the nucleus (with respect to the $e^- - e^+$ mass) the energy absorbed by the nucleus is considered negligible (but not the momentum) and it is assumed that all the energy of the gamma ray is transmitted to the created pair (Bethe-Heitler representation). If the interaction takes place with the electric field of an electron, the energy absorbed by it can be sufficiently high not to be neglected and therefore, as a final result of the process, in addition to the created pair, there is an extra electron (called the recoil electron) constituting what is called a triplet. The probability ratio between the two cases is $1/Z$, therefore one is more likely to observe triples in low Z atoms. Given the high energy of the gamma rays that are usually converted into pairs, the pair created have a very high probability of having very small opening angles (relative to the direction of the gamma ray, polar angle) and this is the same for either of the two processes already mentioned. If the beam is linearly polarized, the direction of the polarization vector is reflected in an asymmetry of the probability distribution of the pair around the axis defined by the direction of the gamma ray (azimuthal angle). This asymmetry is generally small and depends on how far the plane defined by the momentum of the pair moves away from the direction of the gamma ray (coplanarity). This makes the measurement of the asymmetry very dependent on the ability to measure the angles involved ([6], [7], [8]) and it becomes much more difficult for high-energy gamma rays because the polar angles are very small and multiple scattering tends to destroy this information.

In the case of the triplet, it is most probable that one of the three particles has a large polar angle and, with a little less probability, this particle will possess sufficient

energy to be detected using gas detectors ([9], [10]) or Si detectors ([11] [12], [13]) or emulsion technique, [14] making the measurement of polar and azimuthal angles more easier.

The study and analysis of the angular distribution of the electron recoil promises to be an effective method to help to determine the polarization of the gamma ray along with the study of the pair but the indistinguishability of the electrons makes it difficult to identify which is the created electron and which is the electron recoil.

In order to understand and extract the desired parameters, it is necessary to study how this indistinguishability of electrons affects the experimental data.

The momentum (or energy) distributions for the three particles can be calculated by using the standard technique of the quantum electrodynamics in the lower approximation order. For this process:

$$\gamma + e^- = e^+ + e^- + e^-.$$

one has 8 Feynman diagrams, two of them, called the Borsellino diagrams [15] (Ba and Bb in fig. 1), make the main contribution to the total cross section of the process ([16], [17] [1]). Joseph and Rohrlich [16] also show that the process in which the final state configuration consist with the positron and one electron emerging with very high energy is by far the dominant contribution to the cross section.

Many authors put focus only in these diagrams to obtain the momentum or angular distributions of the particle (Boldyshev et. al. [1] made an extensive calculation, for example).

The use of only these two diagrams simplifies the interpretation of the role of the electrons since, according to figure 1, it is clear that p_1 distribution corresponds to the recoil electron and p_2 to the created electron. This is a good approximation for high energy limits that we have established in this work as $\omega \geq 1000m$. This facility is lost when we include the exchange diagrams.

In this work we have shown that for medium and lower energies, the contribution of the other diagrams, in particular the inclusion of the exchange of the Borsellino diagrams overestimate the total cross section making it necessary to take into account all the diagrams (this was also quote by Haug [3]). Also, the probability that the created electron could acquire energy lower than the recoil electron can be significant in the medium and lower regime, and the inclusion of the exchange diagrams change the role of these particles. This is important since in an experiment it is not possible to distinguish between the pair electron and the recoil electron. Our proposal is to calculate the energy distribution in a situation more similar to the experimental setup, that is, to calculate the energy distribution of the lower energetic electron and the energy distribution of the higher energetic electron without taking into account the origin of the electrons.

In section 2, we have given a brief discussion about how we have calculated the cross section from the Feynman diagrams, which variables we have chosen to integrate analytically and which ones, in numerical form, and how to find the limits that the

kinematics has imposed on the variables of interest. The most important diagrams are the Borsellino one and the respective exchange where the labels of the electrons are inverted. We concentrate on the calculations based on these diagrams for explanation.

The section 3 shows the energy distribution given by the different terms of the scattering matrix. We have also tried to show where only the use of the Borsellino diagrams is a good approximation analyzing this overlapping of the distribution that quantifies, in some sense, the probability the role is exchanged between the electrons. In section 3a, we have calculated the energy distribution obtained for the lower energetic electron and for the higher energetic electron in 3b. We have also shown the contribution for many terms of the scattering matrix and compared the sum with the closed formula obtained by Haug [4].

Angular distribution is very important for determining polarization. This is discussed in section 4 for high-energy gamma rays (only Borsellino diagrams were used). It starts from the triple differential cross section and analyzes the distribution of the polar (section 4) and azimuthal angle (section 5) for the different particles and in different regimes of their momenta.

2. Feynman diagrams and some kinematics considerations

The 4-momentum conservation for this collision is written as:

$$k + p = p_r^- + p^- + p^+ = p_1 + p_2 + p_3.$$

As usual, in this work we take \hbar and c equal to 1, and then, in the laboratory system, $k = (\omega, \omega \hat{k})$, and $p = (m, \vec{0})$, where \hat{k} is the unit vector of the incidence γ - ray direction . We call p_1 and p_2 to the 4-momentum of the electrons that, depending on the diagrams, (figure 1) can be the recoil electron or the momentum of the created electron or conversely. p_3 is the 4- momentum of the positron (we use $p_i = |\vec{p}_i|$ for the 3-momentum module).

The cross section of this process can be calculated by using the standard technique. The 8 Feynman diagrams are shown in figure 1, 2 of them, the $B.a$, $B.b$ are the Borsellino diagrams, the other 2, $G.a$ and $G.b$, are called $\gamma - e^-$ and the other 4 ($B_I.a$, $B_I.b$, $G_I.a$, $G_I.b$) are the exchange diagrams due to the indistinguishability between the recoil electron and the electron created (in this last 4th case, the role of p_1 and p_2 interchanges).

Looking at the G diagrams, one can see that these are basically Compton diagrams, with a created pair at the end of the virtual photon, so it is expected that the contributions to the cross section of these diagrams will decrease with the gamma-ray energy.

To illustrate the calculation, we have neglected the G diagrams (however, in our final energy distributuion, we have included all combinations making a total of 10 matrix elements to add). Under these conditions, the matrix elements to be calculated are:

$$|M|^2 = |M_B - M_{BI}|^2 = |M_B|^2 + |M_{BI}|^2 - (M_B M_{BI}^* - M_B^* M_{BI}) \quad (1)$$

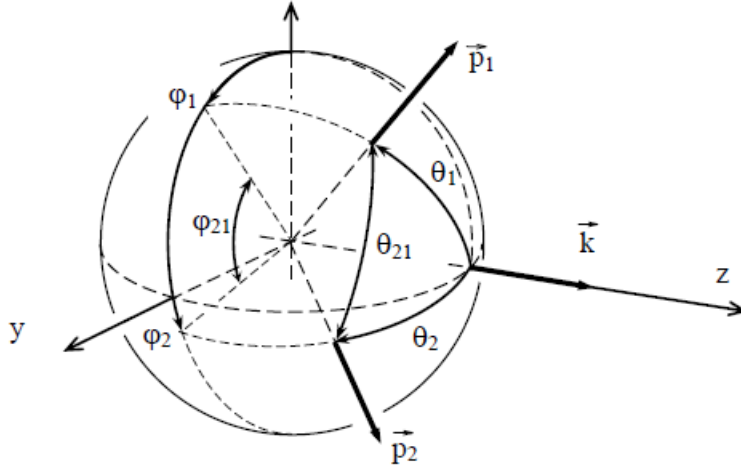


Figure 2: Angles after integrate over positron variables

The first effect to notice with respect to the usual calculations using only the Borsellino diagrams, is the introduction of the term $|M_{BI}|^2$ which consists in the exchange of the label between the two electrons, that is $|M_B(1, 2)|^2 + |M_{BI}(2, 1)|^2$.

The second and the most important contribution is the interference term which give how much overlapping is, in the phase space, between the variables; for example, once one integrate over all the variables except for p_1 ,

$$\frac{d\sigma}{d^3p_1} = \int \int \int |M|^2 \cdots d^3p_2 d^3p_3 \quad (2)$$

one will have the probability density that the recoil electron and the created electron can take the value p_1 .

The inclusion of the exchange term has made it necessary to multiply the cross section by the 1/2 factor to avoid double-counting due to the indistinguishability of the electrons.

The triple differential cross section for the process is:

$$d\sigma = \frac{\alpha r_0^2}{4\pi^2} \frac{1}{\omega m} \frac{d^3\vec{p}_1}{E_1} \frac{d^3\vec{p}_2}{E_2} \frac{d^3\vec{p}_3}{E_3} \delta^4 \left(\sum p_f - \sum p_i \right) \left(\frac{4m^6}{e^6} |M|^2 \right) \quad (3)$$

Since in this work we are interested to describe the electrons distributions, we have used the delta function to integrate over the positron variables (\vec{p}_3),

$$d\sigma = \frac{\alpha r_0^2}{2\pi} \frac{1}{\omega m} \frac{d^3\vec{p}_1}{E_1} \frac{d^3\vec{p}_2}{E_2} \frac{1}{E_3(\vec{p}_1, \vec{p}_2)} \delta \left(\sum E_f - \sum E_i \right) \left(\frac{4m^6}{e^6} |M|^2 \right) \quad (4)$$

where in the M we also must substitute E_3 and \vec{p}_3 by the expressions as a function of \vec{p}_1 and \vec{p}_2 using the conservation law.

The last delta function has been chosen to integrate over the azimuthal angle of electron labeled 2, φ_2 :

$$d\sigma = \frac{\alpha r_0^2}{2\pi} \frac{1}{\omega m} \frac{d^3\vec{p}_1}{E_1} \frac{p_2^2 \sin \theta_2 dp_2 d\theta_2}{E_2 (2\pi p_1 p_2 \sin \theta_1 \sin \theta_2 |\sin(\varphi_2 - \varphi_1)|)} \left(\frac{4m^6}{e^6} |M|^2 \right) \quad (5)$$

The absolute value of the expression corresponds to, once φ_1 is fixed, two possible values to φ_2 that are given by the same θ_{21} (see figure 2). The φ_2 value must void the following expression (where x represents the other variables):

$$g(x, \varphi_2) = \omega + m - E_1 - E_2 - E_3(\vec{p}_1, \vec{p}_2) \quad (6)$$

The condition $g(x, \varphi_2) = 0$ gives the following expression for the $\cos \varphi_{21}$ where $\varphi_{21} = |\varphi_2 - \varphi_1|$:

$$\cos \varphi_{21} = \frac{1}{p_1 p_2 \sin \theta_1 \sin \theta_2} [(\omega + m)(m - E_1 - E_2) + E_1 E_2 + \omega(p_1 \cos \theta_1 + p_2 \cos \theta_2) - p_1 p_2 \cos \theta_1 \cos \theta_2] \quad (7)$$

This expression is not necessarily less than 1 when \vec{p}_1 and \vec{p}_2 are into their validity range given by the kinematics (see figure 3 in ref [18]). Once fixed \vec{p}_1 , this expression is very restrictive to \vec{p}_2 [2]. Defining F as:

$$F = -p_2^2 \cos^2 \theta_2 G + 2p_1 \cos \theta_2 (\omega - p_1 \cos \theta_1) C + p_1^2 p_2^2 \sin^2 \theta_1 - C^2 \quad (8)$$

where:

$$C = (\omega + m)(E_1 + E_2 - m)E_1 E_2 - \omega p_1 \cos \theta_1$$

$$G = \omega^2 + p_2^2 - 2\omega p_1 \cos \theta_1$$

the differential cross section can be written as:

$$d\sigma = \frac{\alpha r_0^2}{2\pi} \frac{1}{\omega m} \frac{d^3 \vec{p}_1}{E_1} \frac{p_2^2 \sin \theta_2 dp_2 d\theta_2}{E_2} \frac{1}{\pi \sqrt{F}} \left(\frac{4m^6}{e^6} |M|^2 \right) \quad (9)$$

where the extreme values of θ_2 (once \vec{p}_1 and p_2 are into their validity range) must satisfy the condition $F \geq 0$

$$\cos \theta_2^\pm = \frac{(\omega - p_1 \cos \theta_1) C \pm p_1 \sin \theta_1 \sqrt{p_2^2 G - C^2}}{p_2 G} \quad (10)$$

(it has been found that the extreme values for θ_2 are very close each other).

The differential cross section (eq.9) admits two analytical integration, one trivial over φ_1 since in any stage of the calculation one can write the cross section as $d\sigma = d\sigma^t - d\sigma^l \cos 2\varphi_1$, the other chosen variable was θ_2 (we have omitted the final expression because it is too long), so finally we have an exact expression for the differential cross section according to $d\sigma = d\sigma(p_1, p_2, \theta_1)$. To obtain the momentum distribution we must continue with numerical integration.

Haug, using another integrating technique, obtained $d\sigma = d\sigma(p_3, \theta_3)$ [3] and $d\sigma = d\sigma(p_2, \theta_2)$ [4] where p_2 and θ_2 are the momentum and polar angle of the electrons (created and recoil), that is, the sum of the each contribution.

In order to test our calculation, in figure 3 we compare the total cross section in function of the threshold momentum (only for the recoil electron) obtained in this work (lines) with the table V in [1] (symbols) obtained using only the Borsellino diagram

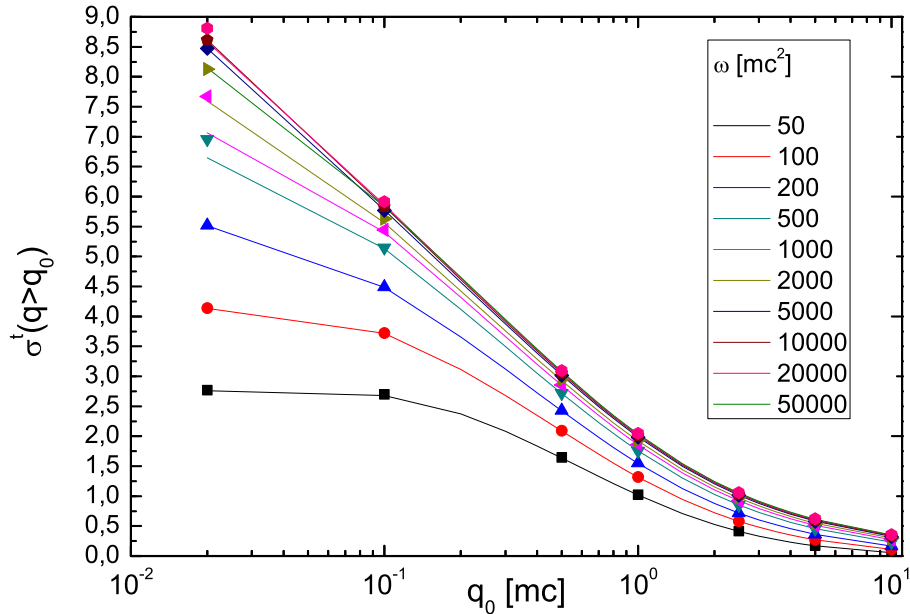


Figure 3: Comparison of total cross section as a function of threshold momentum for many gamma rays energies (lower energy at bottom) between our calculation (line) and table V in [1] (symbols)

in both cases. One can see that for $\omega \geq 5000m$ the curves can not distinguish the asymptotic expression [18] when $q_0 \geq 0.1m$. Bernard [19] also produces these curves including all the terms (figure 6 in [19]) but it is noticed that the values obtained are lower respect to Boldyshev and this work, probably because all the terms have been used (and in this case it is not clear how the threshold is applied).

3. Energy distribution for the electrons

To obtain the energy distribution of p_1 that, as one can see from the Feynman diagrams in fig.1, which represents the recoil electron in $|M_B|^2$ and the created electron in $|M_{BI}|^2$, we have integrate (in numerical form) over $0 \leq \theta_1 \leq \theta_{1max} = \arccos\left(\frac{\omega(E_1 - m) + m(E_1 + m)}{\omega p_1}\right)$ (the maximum θ allowed by the kinematics, eq. 28 in [1]) and over $p_{2min}(\theta_1, E_1) \leq p_2 \leq p_{2max}(\theta_1, E_1)$ (eq.7.3 in [3]), roots of $p_2^2 G = C^2$ (see figure 3 in [18]). Another fact to take into account is that in an experiment there is a threshold for the momentum detection below where the particle is not detected. In our calculations, we have designated to this limit as q_0 and if $p_{min} \leq q_0$ the integration is done between q_0 and p_{max} .

In figure 4 we show the energy distribution for p_1 obtained using only $|M_B|^2$ where it represents the recoil electron and the energy distribution obtained using $|M_{BI}|^2$, where p_1 is the distribution for the electron created in this case. We show the results for 3 different ω , $10m$, $100m$ and $1000m$. As it was mentioned before, the two curves have

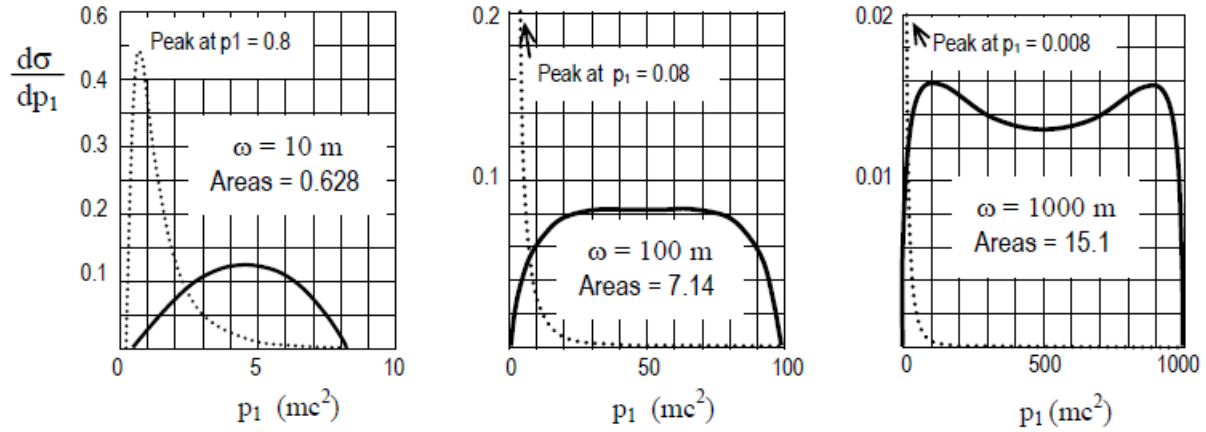


Figure 4: Energy distribution for p_1 obtained using only $|M_B|^2$ where represent the recoil electron and the energy distribution obtained using $|M_{BI}|^2$ only, where p_1 is the electron created in this diagrams.

the same area (shown in the figure and in agreement with that one obtained by Joseph and Rohrlich [16]), the $|M_B|^2$ was truncated to see $|M_{BI}|^2$. The peak of the $|M_B|^2$ is found when $p_1 \simeq 8/\omega$. If the value for the threshold detection for p_1 is around $1m$, in general, only one sees a decreasing distribution for the electron recoil.

From this figure, one can deduce that for $\omega \lesssim 1000m$ the probability that the recoil electron has acquired energy greater than the created electron, is not so small, so to compare the theoretical distribution with the experimental data we propose to calculate $d\sigma_T(p_1 < p_2)/dp_1$ and $d\sigma_T(p_1 > p_2)/dp_1$ ($d\sigma_T$ is the sum of all 10 terms) obtaining in this way the energy distribution for the lower and higher energetic electron whatever their origin is.

3.1. Energy distribution for the lower energetic electron

In the figure 5 we show, for $\omega = 1000m$, the momentum distribution for the lower energetic electron using different contribution of the Feynman diagrams. The symbology used is the following one: B represents the contribution of $|M_B|^2$, BII for $|M_{BI}|^2$, $BI \equiv |M_{BI}M_{BI}^* - M_{BI}^*M_{BI}|^2$, $G \equiv |M_{\gamma e}|^2$ and so on ($GI, GII, BIG, BGI, BG, BIGI$). Figure 5a shows the full scale and one can see how dominant is the $|M_B|^2$ contribution. Figure 5b is the same as figure 4a but with a zoom to see the other contributions. In table 1 we compare the contribution of each term in relation to the areas of each curve respect to the area of the Borsellino term (in percentage) for three gamma-ray energies. It is noteworthy that the only inclusion of the Borsellino exchange diagram imply a correction of 8.15 % for $100m$ and this overestimates the correction that includes all terms, which is 5.88 %.

A better idea about the relation between the Borsellino diagrams and the other terms can be carried out by showing the relation $(d\sigma_B/dp_1)/(d\sigma_X/dp_1)$ (where X

$\omega[m]$	$B[\alpha r_0^2]$	BII	BI	G	GII	GI	BG	$BIGI$	BGI	BIG	Total
100	2.22	3.20	4.95	0.40	1.71	-0.34	-0.48	-0.46	-3.4	-0.62	5.88
1000	3.19	0.67	1.46	0.05	0.36	-0.021	-0.07	0.07	-1.0	-0.07	1.45
10000	3.46	0.11	0.30	0.0057	0.065	-0.0016	-0.0076	0.0077	-0.22	-0.008	0.25

Table 1: Contribution of the matrix terms respect to the Borsellino term (in percent) for three gamma ray energies

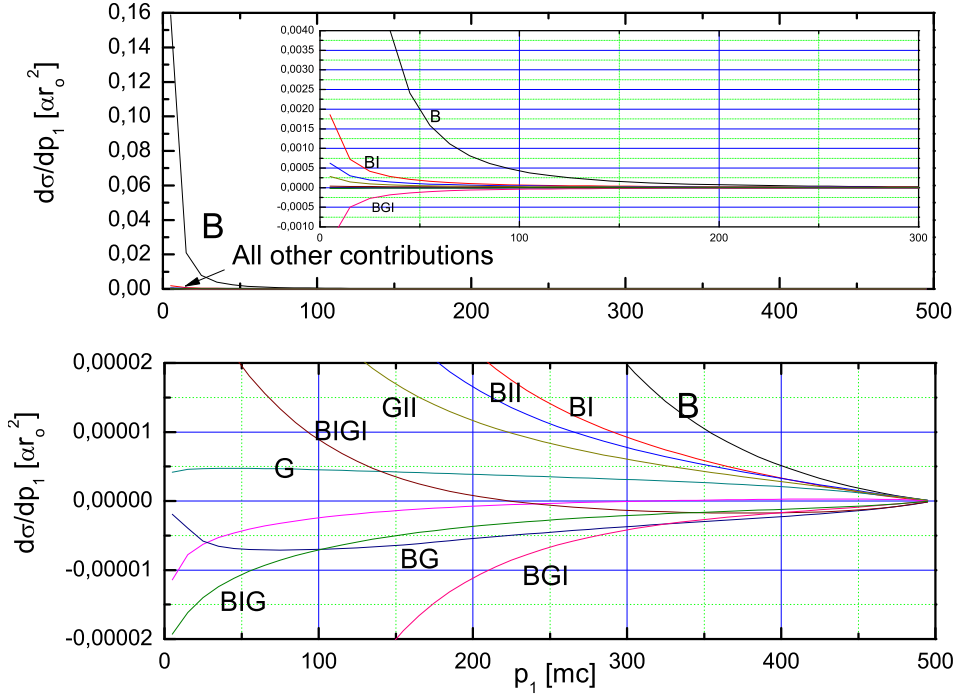


Figure 5: Momentum distribution for the lower energetic electron using different contribution of the Feynman diagram for $\omega = 1000m$.

represents any of the other terms). The results are shown in figure 6 for three different ω and an enlargement in the p_1 scale for $\omega = 1000m$. In this graph, it is possible to see that for lower value of p_1 the curves are seen as a linear function of p_1 (see 6d). Another interesting behavior that one can see is that the axes change very little whereas the abscissa is multiplied by 100, this indicates that the slope in the linear part is proportional to ω^{-1}

Taking into account that the interval of p_1 where the probability is not so small, and does not extend to where ω increases; the zone where the slope is proportional to ω^{-1} does not depend on ω

In this way, the total correction for energy distribution obtained through the Borsellino terms can be written as, with an accuracy of 1%, $d\sigma_{tot}/dp_1 = d\sigma_B/dp_1$ when

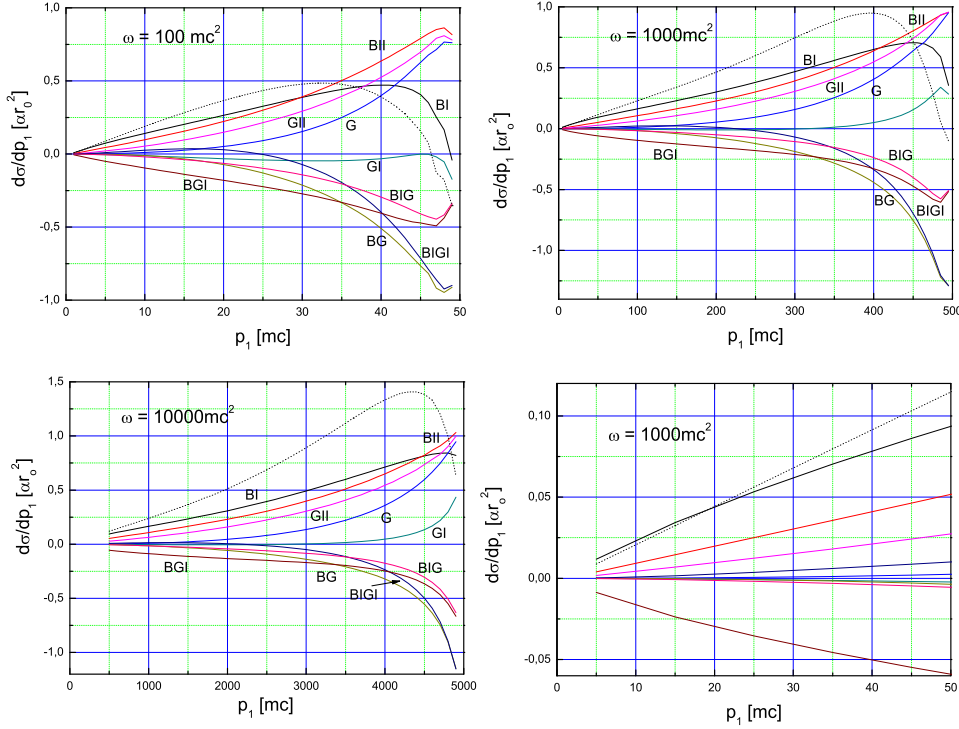


Figure 6: Relation between the Borsellino diagrams and the other terms. The dot line is the sum of all contribution.

$p_1 \leq m$ and for $m \leq p_1 \leq 10m$, so we propose:

$$\frac{d\sigma_{tot}/dp_1}{d\sigma_B/dp_1} = \frac{2.36}{\omega}(p_1 - m) \quad (11)$$

In conclusion, the energy distribution for the lower energetic electron can be expressed as ($m \leq p_1 \leq 10m$):

$$\frac{d\sigma_{tot}}{dp_1} = \frac{d\sigma_B}{dp_1} \left(1 + \frac{2.36}{\omega}(p_1 - m) \right) \quad (12)$$

The next step is to find a handle expression for $d\sigma_B/dp_1$, in this sense one can find in [1] an analytical expression for $d\sigma_{Boldyshev}/dXd\Delta^2$ (eq. 37) where $X = 2m(E_1 - m)$. In the same work, eq. 47 give the integration of eq. 37 over Δ^2 and, with a simple change of variables, can be written in terms of p_1 . The eq. 47 is not very short and it includes the Euler's logarithm but more handled that our numerical integration.

3.2. Energy distribution for the more energetic electron

Now we present the results of the integration over p_2 with the condition that it should be greater than a threshold detection q_0 and lower than p_1 . In figure 7 we compare the obtained distribution taking into account different terms of the matrix for $\omega = 100m$

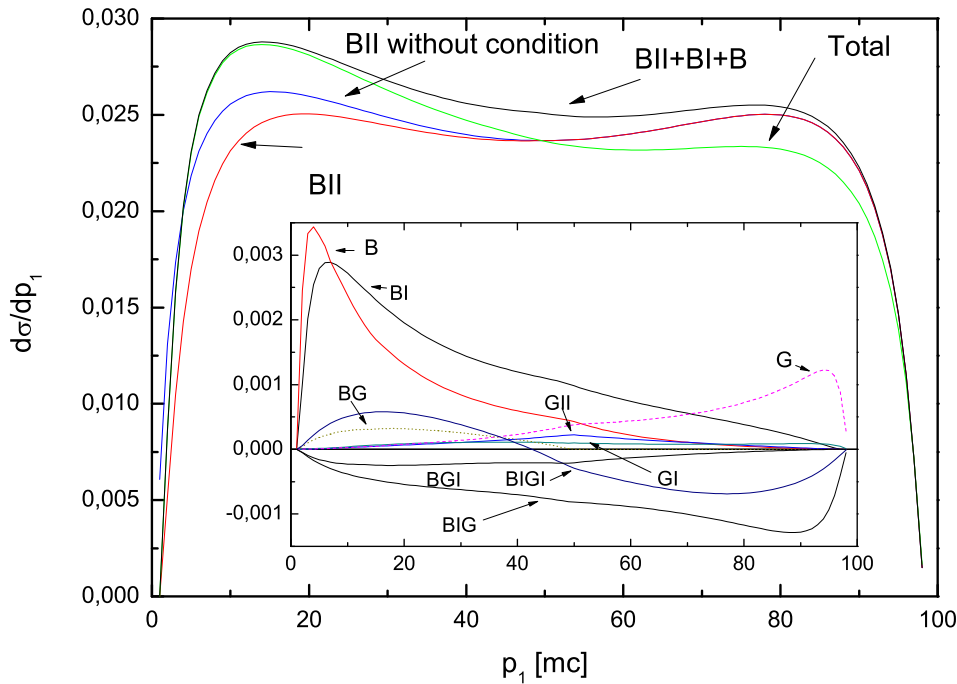


Figure 7: More energetic electron energy distribution, contribution from different terms.

and $q_0 = 1m$. In this graph, one can see that the exchange Borsellino diagrams is dominant and give a curve very symmetric similar to the nuclear case (it can be shown that the BII is similar to the Bethe-Heitler distribution and that for $\omega = 10000m$ it can be indistinguishable between them). In the same figure, we show the curve obtained for the same term without any condition over the momentum; in this case the apparent symmetry is lost and one have more probability in the range lower than $\omega/2$. We also show the other terms, the total (sum of all 10 terms, which represents that one measure in an experiment taken as the most energetic electron like the created electron) and the sum of $BII + BI + B$. One can see that $BII + BI + B$ are the principal contribution but it overestimates the total distribution after the first peak. For $\omega = 1000m$ the difference between this partial sum and the total is 1.5% approximately (it contains more than the 90% of the case). In this case, the main term is BII and one can repeat the same table 1 but, as it is expected, one can obtain the same values by making the following exchange in the notation $B \leftrightarrow BII$, $G \leftrightarrow GII$, $BG \leftrightarrow BIGI$ and $BIG \leftrightarrow BGI$

To analyze the effect of the threshold detection, we have used the BII term in a extreme case, $q_0 = 10m$, as an example since in this term, p_1 is the created electron and p_2 is the recoil electron, and this situation has been assumed in the literature. In figure 8 we compare the momentum distribution obtained for $\omega = 100m$ with the only condition that $p_2 \geq q_0$ (solid line), the condition $p_2 \geq q_0$ and $p_2 < p_1$ (more energetic

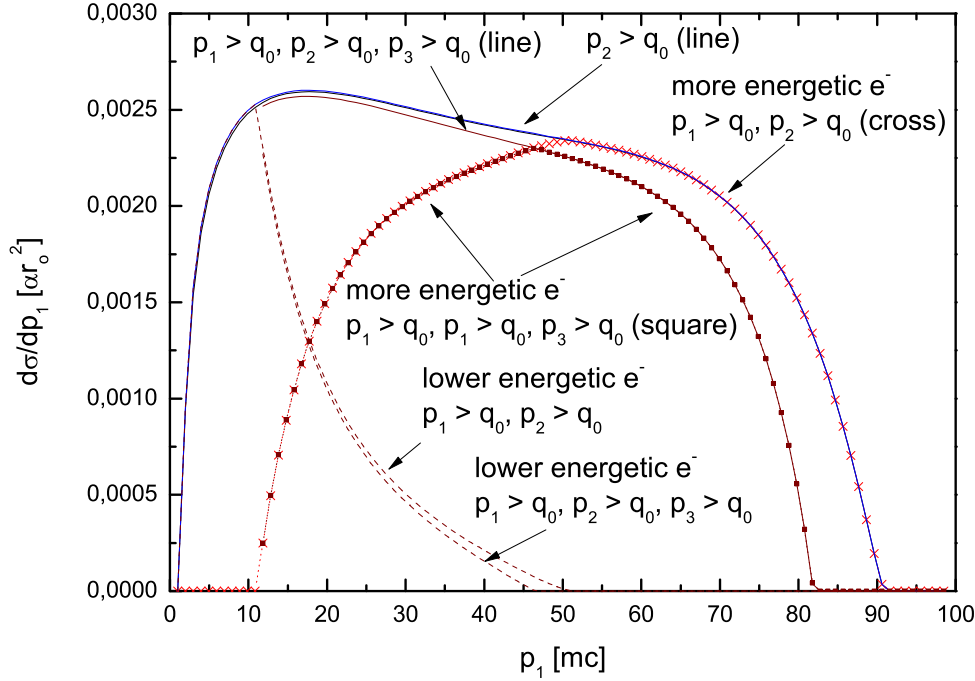


Figure 8: Momentum distribution for $\omega = 100m$ and threshold $q_0 = 10m$ without restriction on the electrons energies (solid line), more energetic electron (dot line) and lower energetic electron (dash line).

electron, dot line) and $p_2 \geq q_0$ with $p_2 > p_1$ (lower energetic electron, dash line). The area of the first one is 0.109mb in agreement with the value obtained by Boldyshev et al (table V in [1]).

Since in the solid curve we only put the threshold on p_2 , one can see that the p_1 distribution has the same form than any threshold (figure 5) in the lower range of p_1 and decreases smoothly until $\geq \omega - q_0$ where it becomes zero ($p_1 \geq \omega - q_0 \Rightarrow p_2 < q_0$).

For the most energetic electron (dot curve) one can see that in the first part it is zero until $p_1 > q_0$ since the condition $p_2 < p_1$ implies we do not have any electron with $p_1 \leq q_0$. For $p_1 \geq \omega - q_0$ it is also zero due to the same reason: the solid curve.

The lower energetic electrons (dash curve) completed, when is added with the more energetic electron, the total momentum distribution. This distribution, without the condition of a threshold for p_2 , show a high peak at $p_1 \simeq 3m$.

If one put the threshold over p_1 the effect is a cut at $p_1 = q_0$ that is $d\sigma/dp_1 = 0$ for $p_1 < q_0$

The positron distribution is obtained in the same way without any condition over the other electrons energies and not using the exchange terms (B and BII produce the same results and they do so with the other case). As was mentioned previously, Haug [3] obtained a close formula for $d\sigma = d\sigma(p_3, \theta_3)$. This formula include all the diagrams.

The figure 13 in the reference [3], show the positron energy distinction for $\omega = 100m$; we reproduce this distribution calculating all the diagrams (6 in this case) and adding them up. From this figure one can see that, contrary to electron, the positron has an average energy greater than that of the electron and for $\omega \gtrsim 200m$ is greater than $\omega/2$, that is, for not so high gamma ray energies, the positron, take more than the half of gamma ray energy, in average. The Haug formula have a maximum that it is easy to parameterize according to the energy of the gamma ray so it can be write a pdf and using the rejection technique one can be sampled, taking into account the kinematics constraints, the energy and polar angle of the positron.

It is reasonable to think that the threshold detection is for the three particles, in figure 8 we show the momentum distribution for the lower and more energetic electron and the total momentum distribution when the threshold detection if for the three particles. The main change is in the high range of p_1 since the distribution reaches $\omega - 2q_0$ because we now have two particles that necessarily take momentum over q_0 . The total cross section for this case is $\sigma(p_1 \geq 10m, p_2 \geq 10m, p_3 \geq 10m) = 0.0533\text{mb}$.

The figure 8 is an extreme case with the objective to make visible the effect; in a more realistic case, $q_0 \ll \omega$, the effect of the threshold can be neglected in the most energetic electrons, and for the lower energetic electron it cuts the events that cannot be detected, modifying only the total cross section, for high gammas-rays energies , the results of $\sigma(q \geq q_0)$ in [24] and part of the table 5 in [1] are valid.

In figure 9 we compare the Haug formula (figure 5 in reference [4]) that include the two electrons with our calculation, in this figure one can see how each term contribute to the total momentum distribution.

In the literature one can find measurements of the energy distribution, for example [20], [21], [22]. Ansoger et al [22] shows the energy distribution in function of $\alpha = (E_+ - E_-)/(E_+ + E_-)$ for 4935 triplets events obtained for gamma-rays energies between 500 – 1000MeV and we compare this experimental result with the asymptotic expression obtained by Wheeler and Lamb [23] (for $q_0 = 1m$) that is very similar to that one obtained by Boldyshev [1]. In figure 10 we reproduce the figure 4 of [22] and we compare it with our distribution obtained for $\omega = 1000m$; to make the comparison, we approximate α parameter of Ansoger as $(E_+ + E_-) = \omega$ so $\varepsilon = (\alpha - 1)/2$.

4. Angular distribution

This section will analyses the angular distribution of triplets produced by very high energy gamma rays. In the previous sections, it was shown that for this regime only Borsellino diagrams predominate and therefore we will only use these diagrams in this analysis.

The kinematics condition between momentum, the polar angle and the invariant mass, express through the relation $p(\theta, \Delta)$ (eq. 14 [1]) play an important role. In figure 11, we plot $p(\theta, \Delta = 2m)$ in logarithmic scale, (we choose $\Delta = 2m$ because the great probability of conversion is for values of very near to $2m$, equal $2m$ means pair with

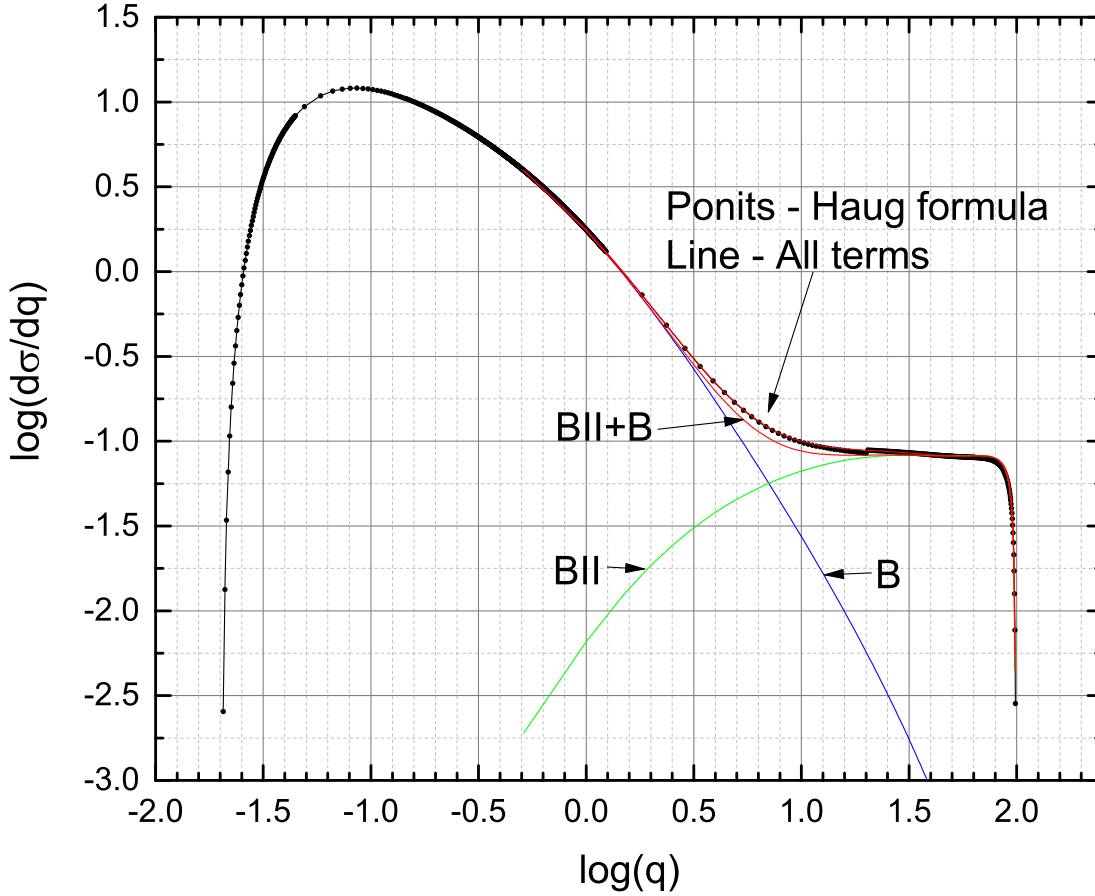


Figure 9: Comparison between Haug formula [4] for electron and our B, BII, B+BII and the sum of the all terms for $\omega = 100m$.

same energies and solid angles) and decrease quickly for values larger than $2m$. We also show a line that represents the $p = 1m$ value to visualize how a threshold detection can affect the maximum angle.

From this figure one can see that large p (in general corresponds to pair created) have small θ , so the transverse component of the momentum can be write as $p_{i\perp} = p_i \sin \theta_i \simeq p_i \theta_i$ ($i = 1, 3$).

We will show that the angular distribution for created pair have a peak at $\theta_i \simeq m/p_i$ so, the transverse component it will expected to be equal to $p_{i\perp} \simeq m$.

In figure 12 we plot the angular distribution for created electron (is equal for the positron) normalized to one for a particular value of p_1 and different regions of p_2 . It is worth mentioning that this distribution is independent of the photon energy. In this figure one can see that the distribution has one peak when $p_2 \ll m$ and this peak is between

$$\theta_{1,3max-prob} \simeq \frac{0.6m}{p_i} \longrightarrow \frac{0.7m}{p_i} \quad (13)$$

and, as a consequence, $p_{1,3\perp} \simeq 0.6m$ to $0.7m$, that is, its is approximately constant and

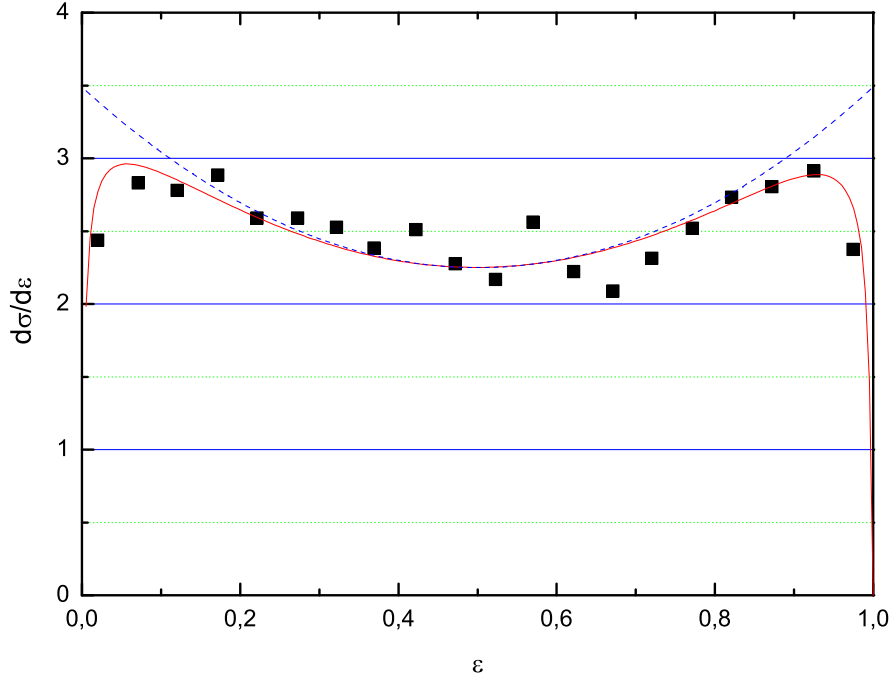


Figure 10: Comparison between experimental data [22] and theoretical calculation for $\omega = 1000m$ and $q_0 = 1m$.

considering that the highest probability is that p_2 is much less than m , this implies that p_1 and p_3 should be approximately perpendicular to p_2 .

Integrating over all possible p_1 values, one finds that the relationship between the maximum polar angle and the energy is $\theta_{max} \simeq m/\omega$ as previously reported.

For $p_2 \gg m$, the angular distribution shows two peaks, one coinciding with the case of $p_2 \ll m$; figure 13 allows us to understand the other peak where the transverse momentum is plotted for $\omega = 1000m$, $p_2 = 50m$ and three values of p_1 . One can see that the peaks do not depend on p_1 and that the second peak is around the $p_1 \simeq 9m$, from figure 10 one can see that the maximum polar angle for this momentum is $\theta_2 \simeq 0.2$ which implies that $p_{2\perp} \simeq 10m$.

This can be interpreted as one of the particles created interacts with the electron of recoil; from this viewpoint, one would expect azimuthal information to be lost. To analyze this, figure 14 graphs the distribution of $\cos\varphi_{31}$ for two cases the p_2 ; a vectorial representation of the transverse momenta is also shown.

From this figure it can be seen that for $p_2 < m$ (the most probable cases) the created pair is approximately coplanar. When $p_2 \gg m$, the φ_{31} angle takes values $< \pi/2$ until θ_1 reaches a value such that $|p_{3\perp}|$ and $|p_{2\perp}|$ are approximately equal, for θ_1 even higher, φ_{31} changes rapidly to values close to π . This also shows that p_1 is always much less

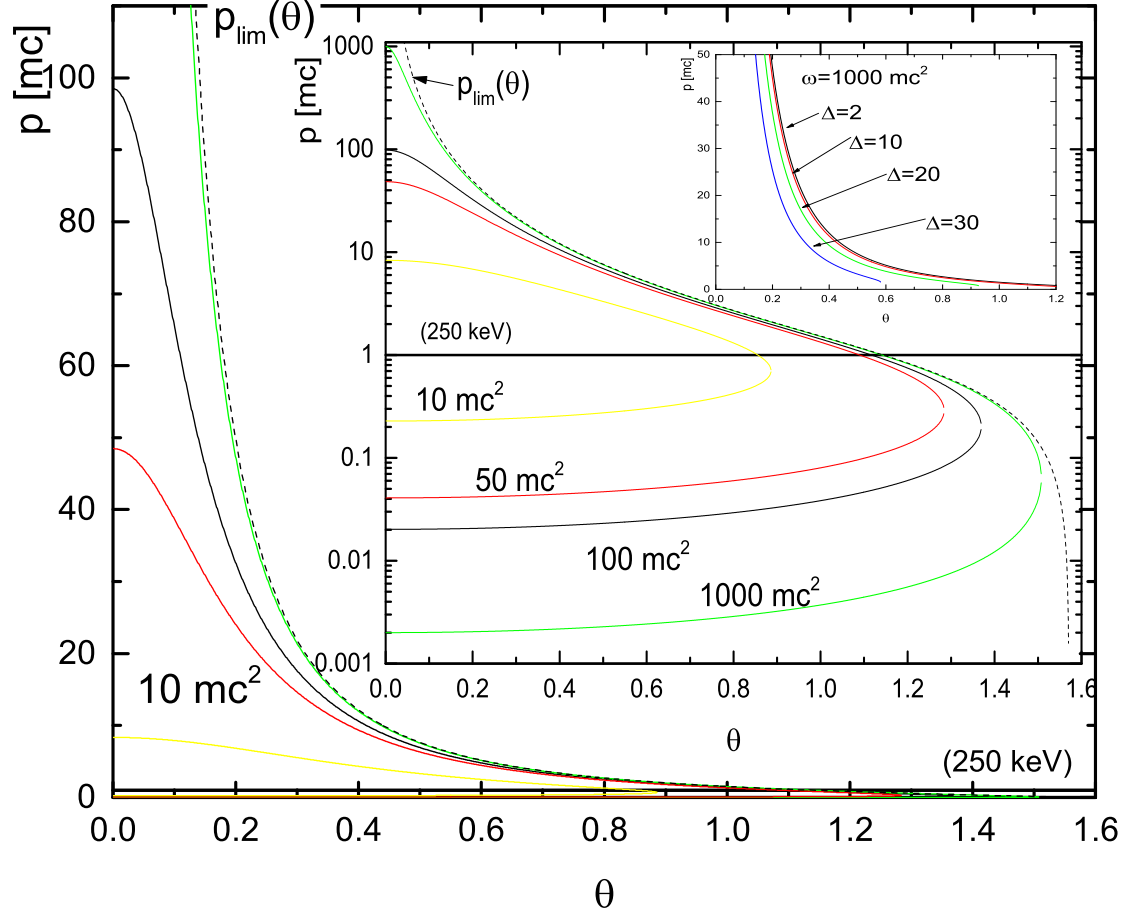


Figure 11: Momentum versus θ for $\Delta = 2m$ and $\omega = 10, 50, 100, 1000m$. Linear scale main graph, log scale inside the graph. Upper right corner: p vs. θ for $\omega = 1000m$ and for $\Delta = 2, 10, 20, 30m$.

than m and that the probability of the 2 particles created interacting with the electron recoil is extremely low.

Figure 15 shows the distribution of θ_1 by integrating p_2 in different ranges. Five curves are shown, four of which integrate p_2 from 0.1 to 1, 5, 10, 30 respectively. The fifth curve is the result of integrating p_2 between 1 and 30. From this figure you can see how the second peak is masked by the low values of p_2 for the high probability that this process has. However, the probability of interaction between the recoil electron and one of the particles created is reflected in the distribution of $\cos \varphi_{31}$.

5. Asymmetry

The cross section can always be written as:

$$d\sigma = d\sigma^{(t)}(\text{variables})[1 + P\Lambda_j(\text{variables})\cos 2\varphi_j] \quad (14)$$

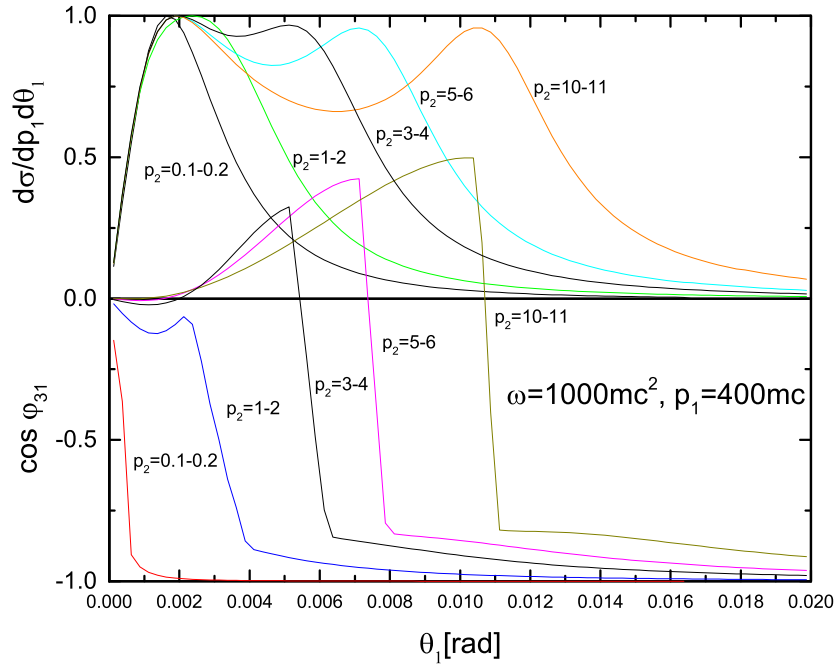


Figure 12: $d\sigma/dp_1d\theta_1$ and $\cos\varphi_{31}$ distribution for $\omega = 1000m$ and $p_1 = 400m$

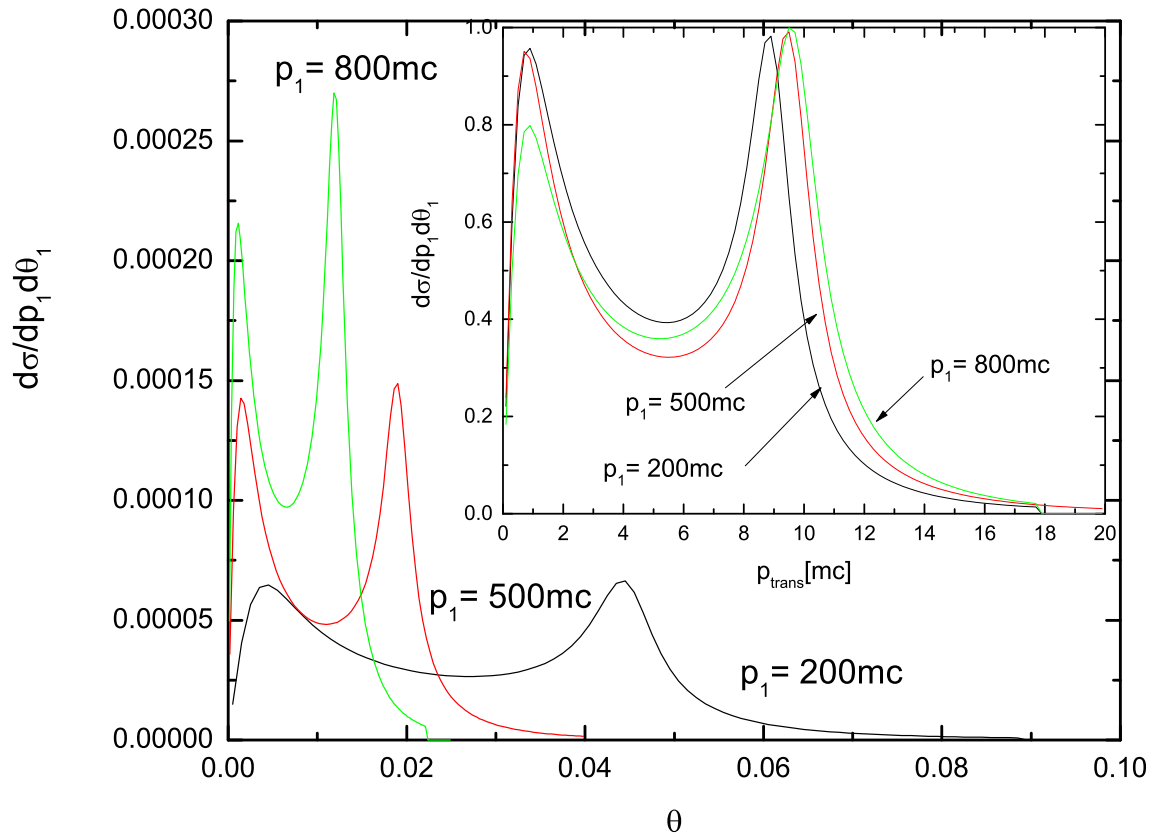


Figure 13: $d\sigma/dp_1d\theta_1$ and transverse momentum plotted for $\omega = 1000m$, $p_2 = 50m$ and three values of p_1 .

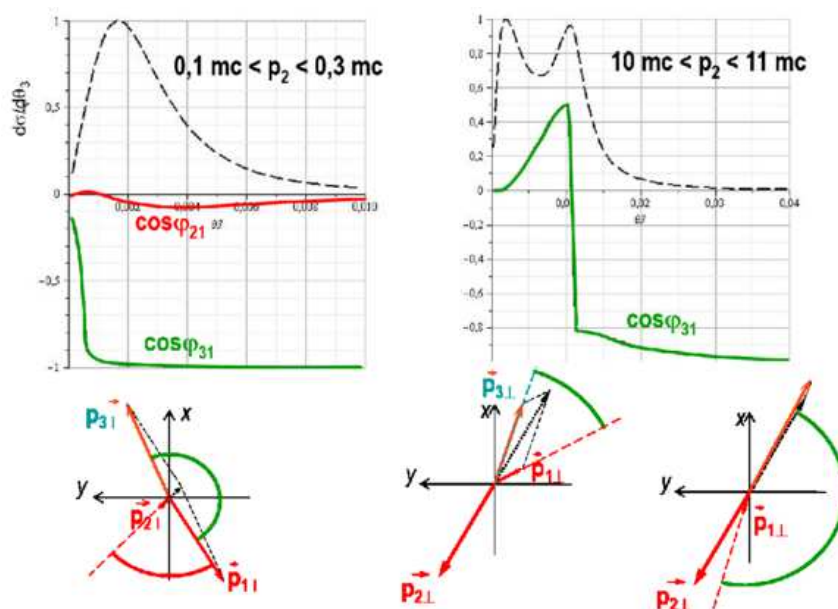


Figure 14: Distribution of $\cos\varphi_{31}$ for two cases the p_2 and a vectorial representation of the transverse momenta

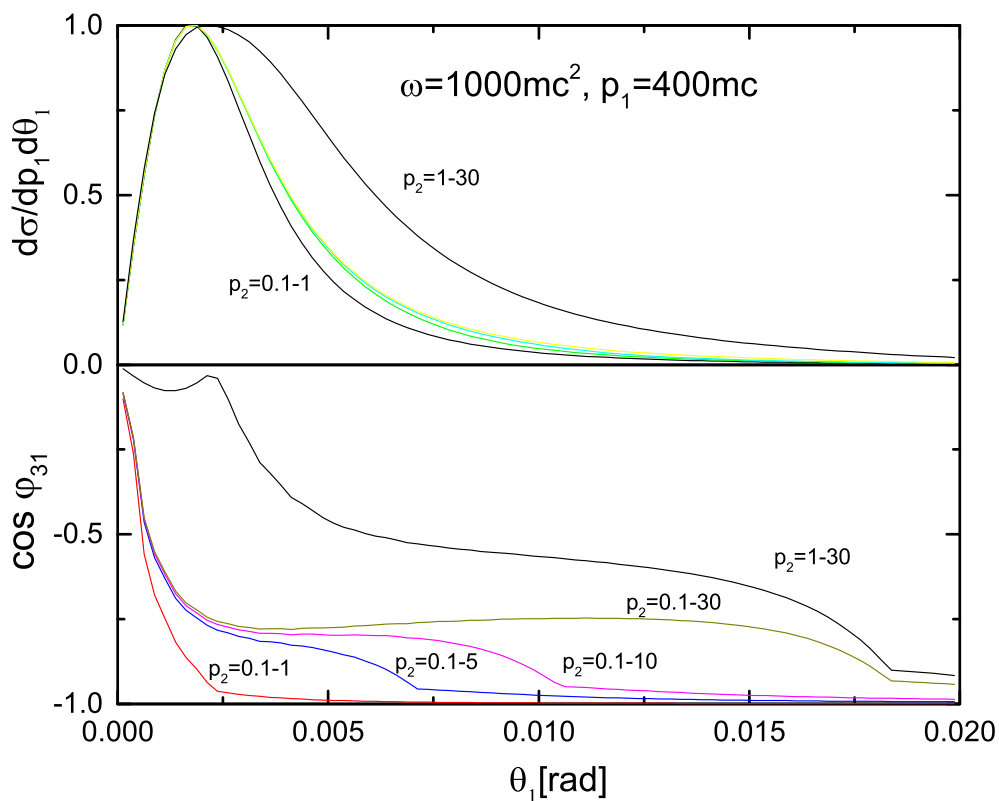


Figure 15: Distribution of θ_1 by integrating p_2 in different ranges indicate in the graph.

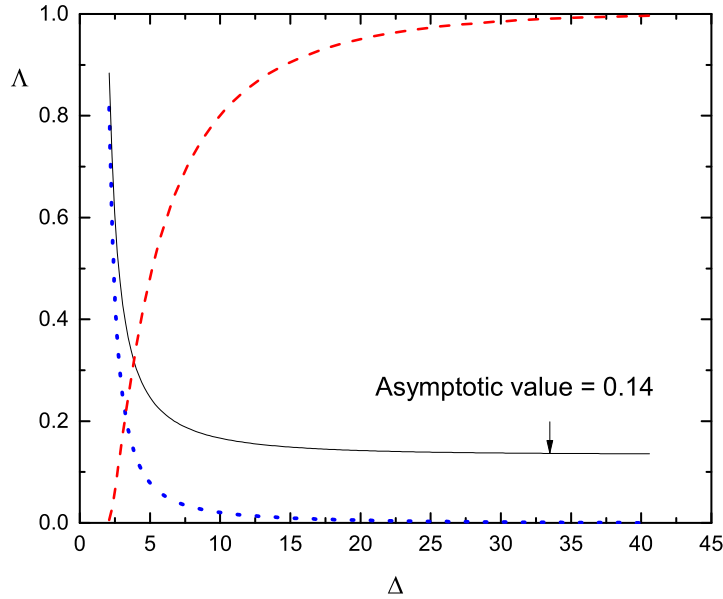


Figure 16: Absolute fraction of triplets as a function of Δ (solid line), fraction of triplets produced up to the value of Δ indicated in the abscissa (dash line) and the asymmetry for each value of Δ (dotted line). The asymptotic value of the table VI of [1] is also shown.

where $j = 1, 2, 3$ are any of the particles and *variables* are polar angles and momenta of any of the three particles but excluding azimuthal angles and the amount goes from none to four, depending on the integration that one can do. In particular, through Boldyshev's [1] equations 37 and 38, one can graph $\Lambda(p_2, \Delta)$ and observe that the asymmetry is maximum for $\Delta = 2m$ and for low values of p_2 .

Figure 16 shows the asymmetry as a function of the absolute fraction of triples produced between Δ_{min} and Δ indicated in the abscissa (solid line) and the fraction of triplets produced up to the value of Δ indicated in the abscissa (dash line). It can be seen that while the asymmetry decreases rapidly when Δ moves away from the value of $2m$ (and reaches the asymptotic value of 0.14), the fraction of triplets increases rapidly. For example, 50% of triplet has $2m \leq \Delta \leq 5m$ and the 80% between $2m \leq \Delta \leq 10m$. The same figure shows the asymmetry for each value of Δ (dotted line), of this curve it can be seen that if only one uses the triplets with $\Delta < 5m$, the asymmetry is around 25% but from figure 11 figure 10 one can see how difficult it is to distinguish Δ from p_2 when $\omega = 1000m$ (making it almost impossible for $\omega = 10,000m$).

Symmetry analysis:

The presence of a second peak in the distribution of the polar angle for large momentum transferred interpreted as a collision between one of the created particles and the electron recoil would indicate that a loss of azimuthal distribution information,

expecting it to become isotropic. Figure 17 shows the asymmetry for one of the particles created and for the recoil electron, for some representative values of ω/p_1 as a function of p_2 . The following conclusions can be drawn from the graph:

1) The Λ_2 asymmetry has a fairly constant negative value for the whole p_2 , this indicates that the electron recoil is placed with greater probability in perpendicular form to the polarization vector and it does it for any value of p_2 and ω .

2) The fact that Λ_2 remains constant at p_2 indicates that the classical interpretation of the collision between two particles and their consequent loss of azimuthal information is invalid. The fact that Λ_2 remains constant for any value of p_2 suggests that the azimuthal location (prior to annihilation) between polarization vector and the electron recoil in whose field the pair is to be produced has an important influence on the matrix elements.

3) The remarkable variation of Λ_2 for $p_2 \ll 0.2$ also does not support a classical interpretation.

4) The Λ_1 asymmetry begins with a large positive value (same order as Λ_2) for low p_2 but decreases with p_2 , cancels and changes sign. This variation if it admits a classical interpretation by thinking that a photon traveling along the z axis with polarization vector along the x axis has a probability of creating a pair greater in the vicinity of electrons close to the plane (z, y) and in the minimum interaction conditions (p_2 lower) the pair is more likely to come out in the plane (x, z) (that is, $\Lambda_1 > 0$); by increasing the intensity of the interaction (p_2 high), the particles of the pair are going to be deviated with more probability in the plane (y, z) , this is $\Lambda_1 < 0$.

6. Conclusion

The work is divided into two parts, on the one hand it analyzes the energy distribution of the 2 electrons present in the final state of the event and due to the indistinguishability of the electrons, we have obtained the momentum distribution for the lower and more energetic electron instead of the recoil or created electron according to a real experimental situation.

We have calculated the 8 Feynman diagrams to take into account all the terms. From the 9 variables that the process has, we have integrate 6 in analytical form and 2 in numerical way to obtain the momentum distribution of one of the electrons. In the calculation, we have taken into account a threshold for the particle detection.

We have tested our formulas calculating the area of the distribution to obtain the total cross section and we have compared it with the results obtained by Joseph and Rohrlich [16], Mork [17] and Haug [3]. Also, we have obtained a very good agreement with the cross section (using only the Borsellino diagrams) as a function of the threshold published by Boldyshev [1] (table V).

For each distribution, we have shown the contribution of each term of the scattering matrix and found that the $G(GII)$ and $BIG(BGI)$ has not neglected contribution for $\omega \lesssim 1000m$ (at $\omega = 1000m$ these terms have a contribution of around 1%).

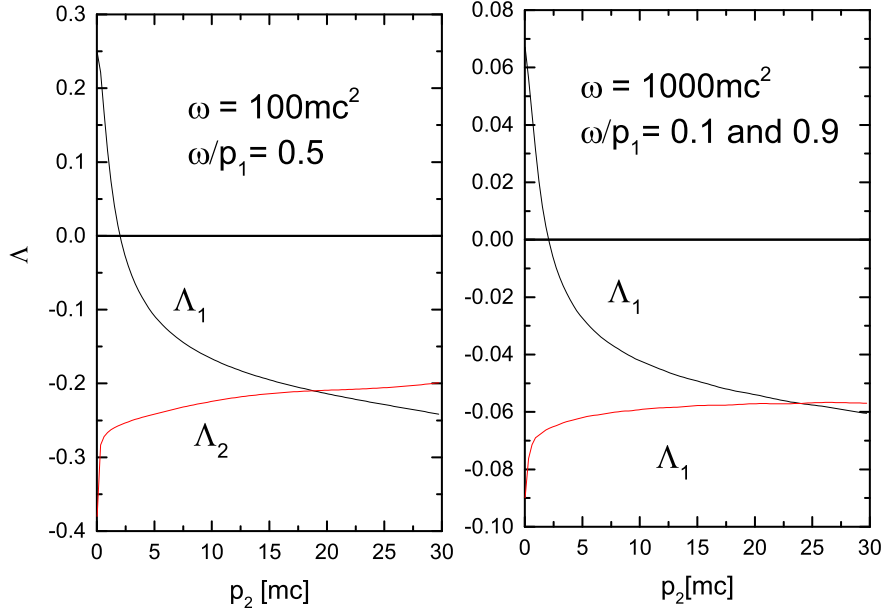


Figure 17: Asymmetry for one of the particles created and for the recoil electron, for some representative values of ω/p_1 as a function of p_2 .

For the lower energetic distribution, we have developed a simple correction of the Borsellino dominant term for this case, B (that can be evaluated more easily using an analytical expression given by Boldyshev [1])

The more energetic distribution (and the distribution for the created electron) show an asymmetry respect to $\omega/2$ (the average energy that the created electron must be $< \omega/2$ since now one have another particles than the electron that must taken energy). As the lower case, $G(GII)$ and $BIG(BGI)$ terms cannot be neglected .

We have shown that the threshold detection for the particles, not only cuts the distributions but also it modifies them, but the modification is not significant when $q_0 \ll \omega$.

Secondly, the angular distribution of particles in their final state was analyzed for the case of high energy (only the terms of Borsellino are used).

It was found that the transverse momentum of the particles created is approximately the same (when there is a low momentum transferred), regardless of the total momentum of the particles and independently of the gamma ray energy.

The distribution of the polar angle shows a peak that is inversely proportional to the total momentum of the particle and for large momenta of transference a second peak appears which, in principle, can be related to an interaction between one of the created particles and the recoil electron.

Furthermore, it was demonstrated that the azimuthal distribution of the electron of recoil is not affected by this interaction (as opposed to what is expected from a collision

from the classical point of view) implying that the previous orientation between the photon (and its polarization vector) and the electron in whose field the pair is produced is an important factor. However, this hypothetical interaction between the two particles is observed in the azimuthal angle between the two particles created.

The asymmetry ratio is increased for pairs of particles with Λ very close to their lower limit but it was shown that selecting these events from the momentum measurement of the electron recoil becomes very difficult for gamma rays with medium large energies and practically impossible for very large energies.

The constancy of the asymmetry Λ_2 and its independence with energy (for energies of high range rays) indicate that this is a better parameter than the asymmetry Λ_1 to determine polarization.

Acknowledgment

The authors would like to thank Prof. Denis Bernard for his invaluable comments and suggestions on this manuscript and Prof. Francesco Longo for their invitations to INFN di Trieste where these ideas were presented and discussed.

References

- [1] V. F. Boldyshev et al. Phys. Part. Nucl. 25, 3 (1994).
- [2] M. L. Iparraguirre. Tesis, Universidad Nacional de Córdoba. 2014 (unpublished).
- [3] E.Haug. Z. Naturforsch 30a, 1099 (1975).
- [4] E.Haug. Z. Naturforsch 40a, 1182 (1985).
- [5] P. Moran et al. Monthly Notices of the Royal Astronomical Society, Volume 456, Issue 3 (2016) 2974.
- [6] G. O. Depaola et al. Astropart. Phys. 10 (1999) 175.
- [7] G. O. Depaola et al. Radiation Physics and Chemistry 53 (1998) 455.
- [8] L.C. Maximon, H.A. Olsen, Phys. Rev. 126 (1962) 310.
- [9] P. Gros et al. Astroparticle Physics 97 (2018) 10 (arXiv:1706.06483).
- [10] S. D. Hunter et al. Astropart. Phys. 59 (2014) 18.
- [11] B. Wojtsekhowski et al. Nucl. Instrum. Meth. A 515 (2003) 605.
- [12] M.Dugger et al. Nucl. Inst. Meth. A 867, 115 (2017)
- [13] A. De Angelis et al. Experimental Astronomy 44 (2017) 25.
- [14] K. Ozaki et al. Nucl.Instrum.Meth. A833 (2016) 165.
- [15] A. Borsellino, Nuovo Cimento 4, 112 (1947). Rev. Univ. Tuc. 6, 37 (1947)
- [16] J. Joseph, Y. Rohrlich. Rev. Mod. Phys. 30, 354 (1958).
- [17] K. J. Mork, Phys. Rev. 160, 1065 (1967).
- [18] G. O. Depaola, M. L. Iparraguirre, Nucl. Inst. Meth. A 611, 84 (2009).
- [19] D. Bernard, Nucl. Inst. Meth. A 729, 765 (2013).
- [20] D. C. Gates et al. Phys. Rev. 125, 1310 (1962).
- [21] E. L. Hart et al. Phys. Rev. 115 678 (1959).
- [22] R. E. Ansoger et al. Phys. Rev. D 7, 26 (193).
- [23] J. A. Wheeler and W. E. Lamb, Phys. Rev. 55, 853 (1939).
- [24] L. Iparraguirre,G. O. Depaola, Eur. Phys. J. C 71, 1778 (2011).